ORIGINAL ARTICLE

Effect of Degree-of-Symmetry on Kinetostatic Characteristics of Flexure Mechanisms: A Comparative Case Study

Xiao-Bing He[1], Jing-Jun Yu[1*], Wan-Wan Zhang[1] and Guang-Bo Hao[2]

Abstract

The current research of kinetostatic characteristics in flexure mechanisms mainly focus on the improvement of accuracy. To reduce or eliminate the parasitic motion is considered as an approach by using the common knowledge of symmetry. However, there is no study on designing the flexure mechanisms with symmetrical features as many as possible for better kinetostatic performance, when considering the resulting cost by the symmetry. In this paper, the concept of degree of symmetry (DoS) is proposed for the first time, which is committed to symmetry design in the phase of conceptual design. A class of flexure mechanisms with 0-DoS, 1-DoS, 2-DoS and 3-DoS are synthesized respectively based on the Freedom and Constraint Topology method. Their overall compliance matrices in an analytical form formulated within the framework of the screw theory are used to analyze and compare the effect of different number of DoS on the kinetostatic characteristics for flexure mechanisms. The finite element analysis (FEA) simulations are implemented to verify the analytical results. These results show that the higher the DoS is, the smaller the parasitic motion error will be. The flexure model with 3-DoS is optimized according to the overall compliance matrix and then tested by using the FEA simulation. The testing result shows that with the best combination parameters, the parasitic motion error for 3-DoS mechanism is almost eliminated. This research introduces a design principle which can alleviate the unwanted parasitic motion for better accuracy.

Keywords: Flexure mechanism, Symmetry, Kinetostatic characteristics, FEA simulation

1 Introduction

Nature can always inspire humans to create various useful devices/instruments. From observing the natural structures and movements of living organisms, mechanical designers regard strategic use of symmetry as a powerful design tool. The symmetrical design in flexure (aka compliant systems) can be found everywhere in nature, from a mirror-symmetry bird wing in the macro world to a large variety of axis-symmetry protein structures in the micro world. Apart from the facts in the natural world, symmetrical geometry also exhibits a wide use in the artificial world. In compliant mechanisms [1], symmetry design is important to guarantee the stability the overall desired performances in which symmetry creates balance, harmony, order, and aesthetically pleasing results [2].

Flexure mechanisms, with the inherent advantages of selective compliance characteristics [3, 4], have been widely used in the field of precision engineering, such as scientific instruments, optical alignment devices, micro-/nano-positioning stages, precision manufacturing machines [5]. These flexure mechanisms are typically hard to design compared to their rigid counterparts. Because the accuracy of flexure mechanisms is highly sensitive to many external disturbances, such as vibration and thermal variations, and also some intrinsic factors, such as material property and mechanism configuration.

In order to formulate an index for accuracy, parasitic motion is defined as any undesirable motion along the constraint directions of a mechanism [6]. There are several methods to reduce and even to eliminate

*Correspondence: jjyu@buaa.edu.cn
[1] School of Mechanical Engineering and Automation, Beihang University, Beijing 100191, China
Full list of author information is available at the end of the article

He *et al. Chin. J. Mech. Eng.* (2018) 31:29

Page 2 of 12

the parasitic motion. The first method is to tune the structural parameters and material properties without changing the type of flexure mechanisms. Li et al. [7, 8] analyzed a family of [PP]S parallel mechanisms and took the 3-PRS parallel mechanism as an example to reveal the relationship between structural parameters and parasitic motion, and then showed the necessary structural condition for a 3-PRS parallel mechanism without parasitic motion. However, it is rather difficult to eliminate the parasitic motion by optimizing the geometrical parameters. The second one is designing a parasitic-motion compensation module, as done in linear-motion flexure mechanisms [9]. Trease et al. [10] and Cannon et al. [11] constructed a linear-motion flexure mechanism with higher accuracy by mirroring two double-parallelogram flexure modules. A class of compliant Roberts mechanisms can also be combined both in serial and parallel to compensate for the parasitic motion [12]. In respect to the multi-axis motion mechanism, an extended parasitic motion compensation approach that characterizes 3D flexure deformations with twists and parasitic error with compliance elements is proposed to synthesize multi-axis flexure mechanism [13]. It is noted that symmetry design is essentially a special case of the latter method, which is to design a system free of parasitic motion directly. Several practical full-symmetrical compliant mechanisms have been studied by Hao et al. [14–16], in which tri-symmetrical planar structures enabled three large-range out-of-plane motions.

This paper aims to explore the method of parasitic motion free design with aid of the knowledge of symmetry. A new term named as the Degree of Symmetry (DoS) is coined for advancing systematical design, with a particular emphasis on type synthesis of flexure mechanisms. It can be argued that synthesis of flexure mechanisms is more difficult than that of their rigid-body counterparts. Therefore, the attempt in this paper is to design a group of specific flexure mechanisms with one rotational degree-of-freedom (DOF) and one translational DOF that are parallel to each other. Each one is composed of several beams uniformly contained in two planes. Based on the known methodology, in this paper a class of flexure mechanisms with different DoS are to be synthesized, and further to be used to identify the relationship between the number of symmetrical planes and their kinetostatic performance characteristics.

In fact, there exist a dozen of literatures about symmetry design, but few design concerns towards how much the symmetry obtained can provide better performance. In these prior art, researchers generally design a class of symmetrical flexure mechanisms firstly, and then analyze their parasitic motions, and finally draw a conclusion that the symmetry design can effectively improve accuracy

and other performances. Is it necessary to design the flexure mechanisms with symmetrical planes, axes, or points as many as possible for reducing or even eliminating the parasitic motion, when considering the resulting cost by the symmetry? This paper will focus on the effect of the DoS on the kinetostatic characteristic of flexure mechanisms with a comparative case study.

The rest of this paper is organized as follows. Section 2 provides an introduction to the Freedom and Constraint Topology (FACT) method as well as the equivalent constraint model of selected flexure primitive within the framework of the screw theory. A group of 2-DOF flexure mechanisms with X-DoS are synthesized by using the graphic method (FACT) in Section 3. Their overall compliance matrices for evaluating parasitic motions are formulated, followed by the FEA simulation in comparisons with the analytical models in Section 4. Based on the forehead context, Section 5 discusses the effect of DoS on the kinetostatic performance. Finally, conclusions are drawn (Additional file 1).

2 Theoretical Foundation
2.1 Definition of Degree-of-Symmetry
Symmetry is one of the most important of all properties in the identification of mechanisms. It is well known that symmetry is always described by reference to symmetry planes, axes and the center of symmetry. In this paper, the Degree-of-Symmetry (DoS) is specifically constrained with plane symmetry.

A plane of symmetry is an imaginary plane that bisects a structure into halves, which is a mirror image of the other. It is a symmetry of a pattern in the Euclidean plane. For a flexure mechanism, it can have one or more planes of symmetry. Thus, the Degree-of-Symmetry reflects the number of planes of symmetry in the mechanism. For example, 1-DoS mechanism means there is only a plane of symmetry and it can be *XY*-plane, *YZ*-plane or *ZX*-plane when the mechanism is placed in the Cartesian coordinate system. The visualization of DoS is shown in Figure 1.

2.2 Type Synthesis Approach
As well known, some systematic approaches including the constraint-based design method [17] and the Freedom and Constraint Topology (FACT) method [18], have gained a great success in the design field of flexure mechanisms. Using the graphic FACT approach, which is based on the connection of screw theory with the constraint-based design theory in a geometrical way, is very powerful for designing simple cases. It has clear meaning to map geometrical entities such as lines and plane, to physical elements such as the compliant beams. Furthermore, all of them can be included in the chart of FACT,
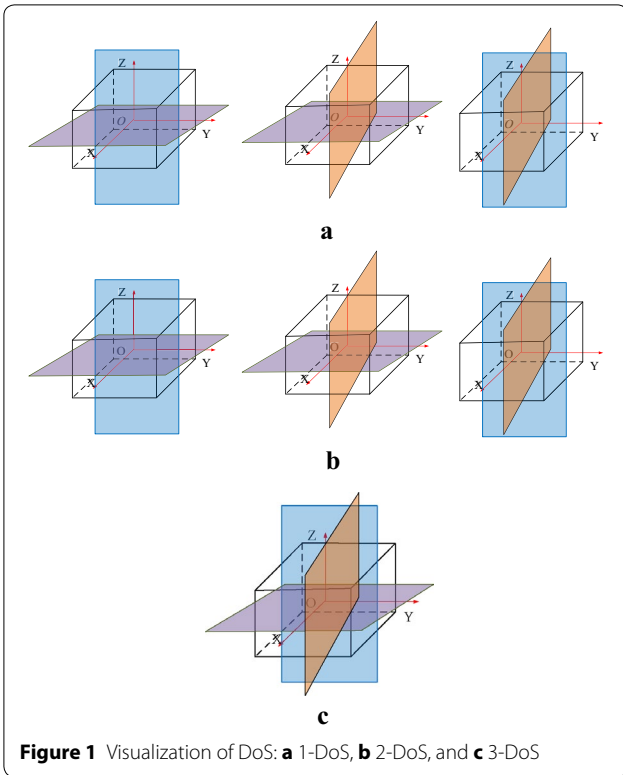
He *et al. Chin. J. Mech. Eng.* (2018) 31:29

Page 3 of 12

Figure 1 Visualization of DoS: **a** 1-DoS, **b** 2-DoS, and **c** 3-DoS

and modelled in the freedom spaces or constraint spaces. In this regard, a freedom space of a rigid body represents all of its allowable motion in space when subjecting to a specified constraint arrangement. While the constraint space represents all possible constraint arrangements in such a prescribed motion pattern.

What is more significant, the FACT approach can be completely embedded into the framework of screw theory, making the compliance matrix characterized by screw theory more powerful [19], since it offers critical geometric insight into various motion behavior of flexure mechanisms, including the metrics quantifying parasitic motion of flexure mechanisms [20].
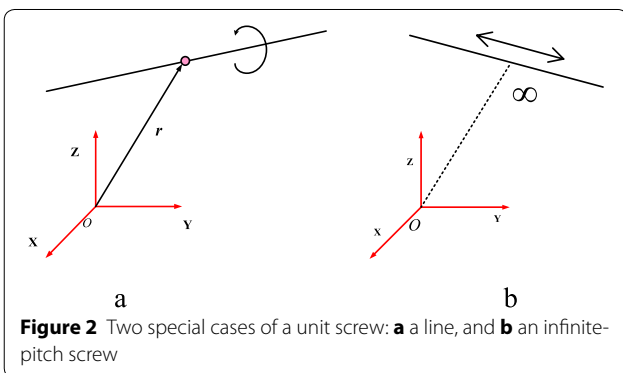

Figure 2 Two special cases of a unit screw: **a** a line, and **b** an infinite-pitch screw

2.3 Coordinate Transformation of Screws and Compliance Matrix

Screw theory underlies the foundation of both instantaneous kinematics and statics [21]. Physically, a unit zero-pitch screw presents a pure rotation or a revolute pair in kinematics, or a unit pure force in static along the line in space. A unit infinite-pitch screw denotes a pure translation or a prismatic pair in kinematics or a pure couple in statics, as shown in Figure 2. One calls a screw a twist if it represents the instantaneous motion of a rigid body, and a wrench if it denotes a system of forces and couples acting on the rigid body. Surely, a wrench and a twist can be also used to describe the motion of a rigid body supported by a compliance structure.

When a load is applied on the functional body of a general flexure mechanism, as shown in Figure 3, it will generate some specified deformation or motion. In this paper, it is assumed that the deformation is sufficient small so that the linear elastic theory can apply.

In this context, the transformation between a deformation twist $\boldsymbol{\xi} = (\boldsymbol{\theta}; \boldsymbol{\delta}) = (\theta_x, \theta_y, \theta_z; \delta_x, \delta_y, \delta_z)^{\mathrm{T}}$ and the load wrench $\boldsymbol{F} = (\boldsymbol{\tau}; \boldsymbol{f}) = (\tau_x, \tau_y, \tau_z; f_x, f_y, f_z)^{\mathrm{T}}$ is represented by a 6×6 compliance matrix $\boldsymbol{C}$ to formulate the mapping of compliance, written as

$$\boldsymbol{\xi} = \boldsymbol{CF}. \tag{1}$$

However, compliance matrices may undergo a transformation representation when calculating the overall compliance matrix of a flexure mechanism. This requires the
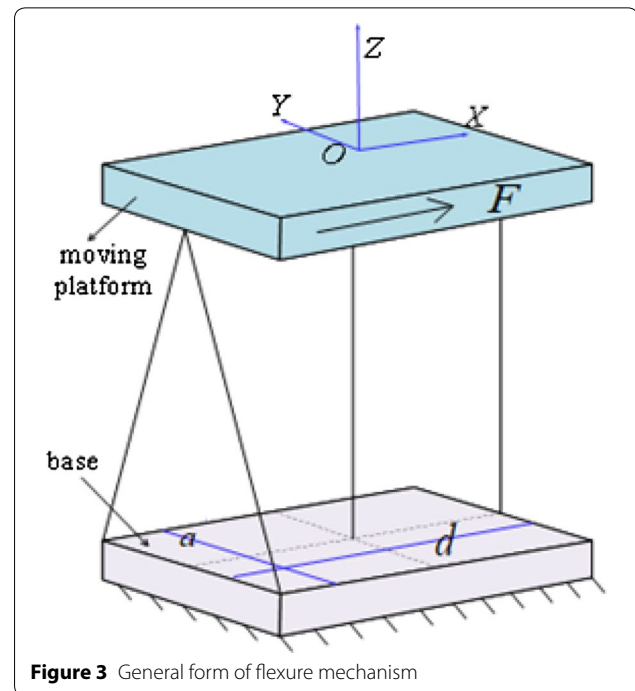

Figure 3 General form of flexure mechanism

He *et al. Chin. J. Mech. Eng.* (2018) 31:29

Page 4 of 12

compliance matrices of all flexures to be implemented in a uniform coordinate frame. Let $\boldsymbol{\xi}$ and $\boldsymbol{F}$ be the twist and the wrench with respect to a global coordinate frame, while $\boldsymbol{\xi}'$ and $\boldsymbol{F}'$ be the twist and the wrench with respect to a local coordinate frame. For a general Euclidean change of coordinate, and suppose that the coordinate transformation is represented by a 3×3 rotation matrix $\boldsymbol{R}$ and a translation vector $\boldsymbol{t} = (x, y, z)^{\mathrm{T}}$, an adjoint representation [Ad] between a local coordinate frame and a global one, the transformation matrix, is determined by

$$[\mathrm{Ad}] = \begin{bmatrix} \boldsymbol{R} & \boldsymbol{0} \\ \boldsymbol{TR} & \boldsymbol{R} \end{bmatrix}, \tag{2}$$

where $\boldsymbol{T}$ is a 3×3 skew-symmetric matrix defined by the translation vector $\boldsymbol{t}$.

Thus, the compliance matrix $\boldsymbol{C}$ with respect to the global coordinate frame can be finally obtained as:

$$\begin{aligned} \boldsymbol{\xi} &= [\mathrm{Ad}]\boldsymbol{\xi}' = [\mathrm{Ad}]\boldsymbol{C}'\boldsymbol{F}' = \boldsymbol{C}\boldsymbol{\Delta}[\mathrm{Ad}]\boldsymbol{\Delta}\boldsymbol{F}', \\ \boldsymbol{C} &= [\mathrm{Ad}]\boldsymbol{C}'[\mathrm{Ad}]^{\mathrm{T}}, \end{aligned} \tag{3}$$

where $\boldsymbol{\Delta}$ is an operator for transforming the axis coordinate into the ray coordinate and $\boldsymbol{C}'$ is the compliance matrix with respects to the local coordinate frame.

Calculation of the resultant compliance of a general flexure mechanism with serial, parallel or a hybrid topology is different. For a serial flexure mechanism, the deformation of the end-effector is the superimposition of the deformation of individual elements. When the compliance of the ith flexure element is denoted by $\boldsymbol{C}_{si}$, the overall compliance matrix of a serial flexure mechanism is calculated as

$$\boldsymbol{C}_{\mathrm{s}} = \sum_{i=1}^{m} [\mathrm{Ad}_i]\boldsymbol{C}_{si}[\mathrm{Ad}_i]^{\mathrm{T}}, \tag{4}$$

where $[\mathrm{Ad}_i]$ is the coordinate transformation operator from the ith flexure to the global frame.

For a parallel flexure mechanism, the overall stiffness matrix of a parallel flexure mechanism $\boldsymbol{K}_{\mathrm{p}}$ is the sum of individual element stiffness in the same coordinate frame, calculated as

$$\boldsymbol{K}_{\mathrm{p}} = \sum_{j=1}^{n} \left([\mathrm{Ad}_j]\boldsymbol{C}_{pj}[\mathrm{Ad}_j]^{\mathrm{T}} \right)^{-1}, \tag{5}$$

where $\boldsymbol{C}_{pj}$ denotes the compliance of the ith flexure element (Additional file 1).

In an overall compliance matrix, the principle diagonal elements are always considered as the reference of rotational degrees of freedom about x, y and z-axes as well as the reference of translational degrees of freedom along x, y and z-axes [22]. Other non-principal diagonal

compliance elements can be used to indicate the parasitic motion [23].

2.4 Equivalent Constraint Model of Flexures

In the family of flexure mechanisms, a beam is widely used as a basic flexure element both generating twist deformations and providing wrench constraints. In terms of the difference in profiles, the beams can be classified as notch-type ones (such as circular flexures) and uniform ones (such as wire flexures, plate flexures); straight ones and initial-curve ones; and slender ones (Euler–Bernoulli beams) and short ones (Timoshenko beams). Different profiles of these beams definitely lead to variance in freedom and constraint due to their compliance properties.

As shown in Figure 4, when the cross section of a beam is circular, the coordinate frame is located at its centroid C, and the compliance matrix of the uniform wire beam with the length l and the radius r of cross sections can be written as

$$\boldsymbol{C}_{\mathrm{c}} = \mathrm{diag}\left[\frac{l^3}{12EI_y} \quad \frac{l^3}{12EI_x} \quad \frac{l}{EA} \quad \frac{l}{EI_x} \quad \frac{l}{EI_y} \quad \frac{l}{GJ} \right], \tag{6}$$

where $A = \pi r^2$, $I_x = I_y = \pi r^4 / 4$, $J = I_x + I_y = \pi r^4 / 2$.

By comparing the compliances of the wire flexure with circular cross section in different directions, the equivalent constraint model can be established for realizing the simplification from structure to topology. When ratio of the length to the radius is larger than 40, we have

$$\frac{c_{c11}}{c_{c33}} = \frac{c_{c22}}{c_{c33}} = \frac{l^3}{12EI_y} \bigg/ \frac{l}{EA} = \frac{1}{3}\left(\frac{l}{r}\right)^2 = 133,$$

$$\frac{c_{c44}l^2}{c_{c33}} = \frac{c_{c55}l^2}{c_{c33}} = 1600, \quad \frac{c_{c66}l^2}{c_{c33}} = \frac{2l^2}{3(1+\mu)r^2} \geq 1000. \tag{7}$$

From the above results, it can be observed that this flexure offers several orders of magnitude higher stiffness

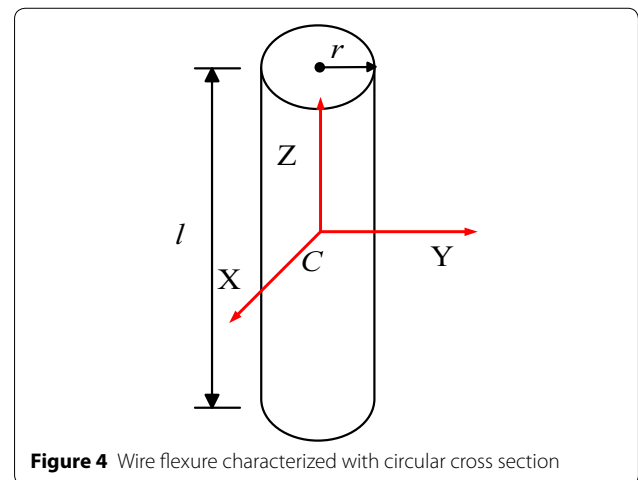**Figure 4** Wire flexure characterized with circular cross section

He *et al. Chin. J. Mech. Eng.* (2018) 31:29

Page 5 of 12

along its axis compared with any other direction. We can thus conclude that a slender cylinder flexure, with ratio of the length to the radius being larger than 20, approximates an ideal wire flexure imposing a rigid constraint along its z axis and allowing other five DOFs. Therefore, the constraint model equivalent to this kind is a wire constraint.

3 Type Synthesis and Parasitic Error Analysis of X-DoS Flexure Mechanisms with Cylindrical Motion

3.1 Type Synthesis

In this section, we deal with the design of a group of flexure mechanisms characterized by the different number of DoS. The type synthesis approach we used is the graphic FACT, which is intuitively visible and preferable if the cases are not so complicated. Since the main purpose to this paper is on the relationship between the number of DoS and the kinetostatic performances, some simple parallel flexure mechanisms are appropriate enough in certain sense. Moreover, all flexure elements employed here are identical with a uniform circular cross section for convenience. Based on the knowledge of equivalent constraint model above, we built a general flexure mechanism formed by connecting a moving platform to a base one through wire flexure elements, as shown above in Figure 3, which will generate deformation on the moving platform when undergoing a generalized load.

Type synthesis of flexure mechanisms starts with specifying a freedom space. The objective is to find all beams with circular cross section in a parallel arrangement to perform the desired motion. The following will describe a general procedure for the type synthesis by taking the flexure mechanisms with cylindrical motion for instance.

Step 1. Denote the specified freedom pattern of a flexure system with one rotational motion and one translational motion whose axes are parallel to each other. The freedom space is depicted in Figure 5.

Step 2. Find the complementary line constraint space, which represents those available constraints of the flexure systems, based on the chart of FACT, as illustrated in Figure 6.
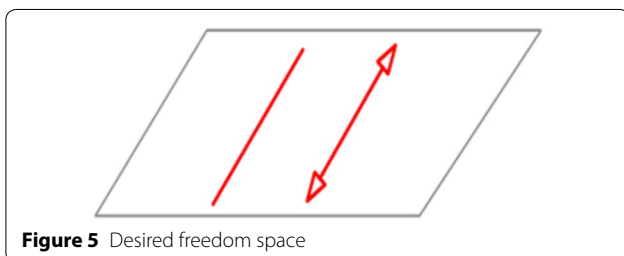
Step 3. Determine all possible reciprocal line subspaces. In the subspaces, an axis is set up to have the identical direction with that of the desired DOFs, and constraints of the flexure systems should be found in an easier way. One possible constraint subspace is illustrated in Figure 7.

Step 4. Select constraint subspace types in terms of different level of symmetrical geometry from constraint spaces obtained in Step 3. Note that the constraint subspaces should be realized physically as illustrated in Figure 8.

Note that the flexure mechanisms constructed based on the above steps can be classified into four types, i.e., 0-DoS type, 1-DoS type, 2-DoS type, and 3-DoS type, as shown in Figure 8. Generally, when formulating the screw-based compliance models, the global coordinate system is placed at the mass center of the moving platform where an important geometrical insight into
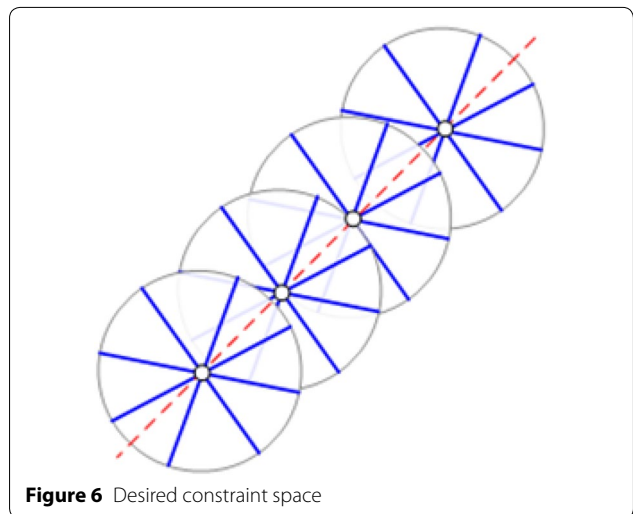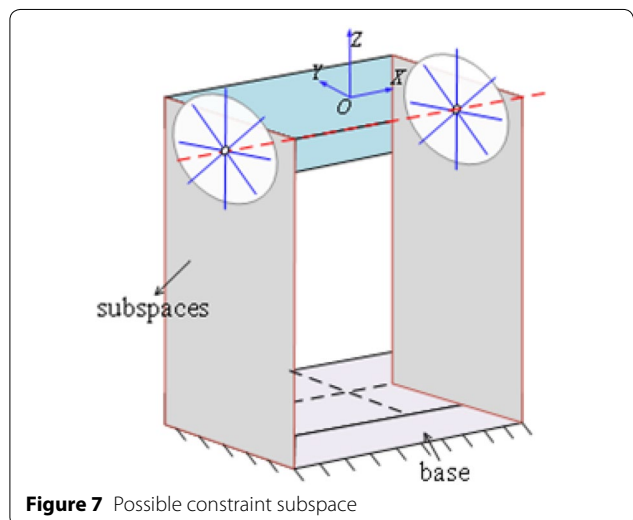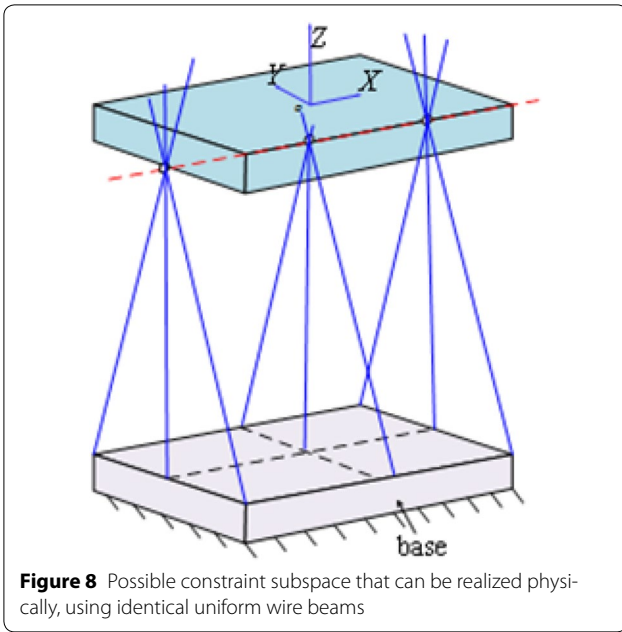

Figure 6 Desired constraint space
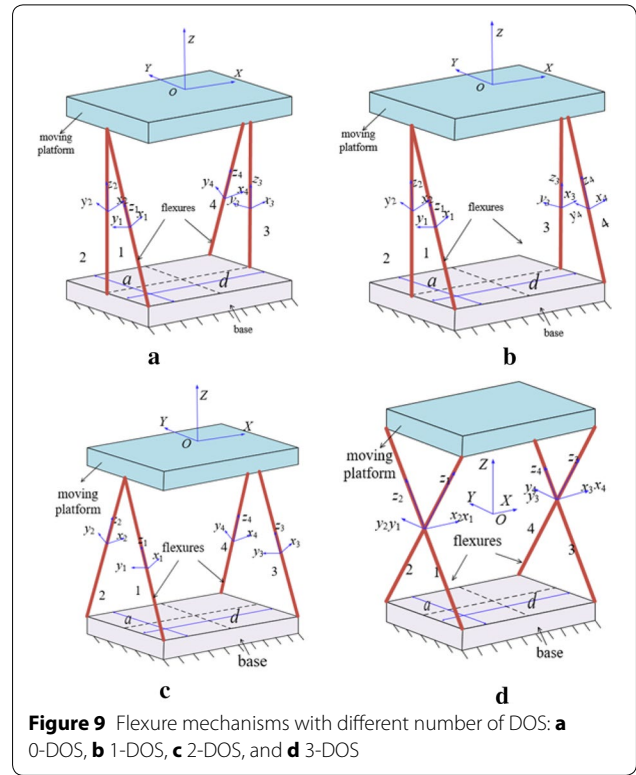

Figure 7 Possible constraint subspace

Figure 5 Desired freedom space

He *et al. Chin. J. Mech. Eng.* (2018) 31:29

Page 6 of 12

Figure 8 Possible constraint subspace that can be realized physically, using identical uniform wire beams

Figure 9 Flexure mechanisms with different number of DOS: **a** 0-DOS, **b** 1-DOS, **c** 2-DOS, and **d** 3-DOS

the motion characteristic of flexure mechanisms can be revealed. However, instead of designing a hybrid flexure mechanism, by applying a mirror-symmetrical serial connection, the global coordinate system is located at the middle part between the moving platform and the fixed platform for the 3-DoS flexure mechanism. All four mechanisms have been elaborated in Figure 9.

3.2 Compliance Modelling

As sketched in Figure 9(c), the flexure mechanism characterized by two symmetrical planes is formed by connecting a moving platform to a fixed one through four identical circular wire flexures (r is the radius of cross sections) in parallel. Two parallel flexures (labeled with 1 and 2) intersect, with an angle 2θ, at the middle of one side edge on the moving platform, and span, with the distance a of two end points, on the fixed platform. The other two flexures are arranged similarly with an interval distance d. A global coordinate frame is located at the center of the moving platform, and the local coordinate frames are located at the center of each flexure element. All axes of the local/global coordinate frames are labeled in Figure 8.

Note that the compliance of each element can be obtained under the uniform coordinate frame although the compliance matrix about each flexure center, which has deduced in Eq. (6), is identical. The rotational matrices R_i and the translational vector $t_i = (x, y, z)^\mathrm{T}$ associating with each flexure for calculating adjoint transformations [Eq. (2)] are listed in Table 1, the rotation matrices are expanded as below:

$$R_x(\theta) = \begin{bmatrix} 1 & 0 & 0 \\ 0 & \cos\theta & -\sin\theta \\ 0 & \sin\theta & \cos\theta \end{bmatrix}, \ R_x(-\theta) = \begin{bmatrix} 1 & 0 & 0 \\ 0 & \cos\theta & \sin\theta \\ 0 & -\sin\theta & \cos\theta \end{bmatrix},$$

where $\theta = 0$ if the flexure elements are perpendicular with two platforms.

Based on Eqs. (2) and (3), the corresponding overall compliance matrix of the 2-DoS flexure mechanism with respect to the global coordinate frame is derived as

$$C_{2-\mathrm{DOS}} = \left(\sum_{i=1}^{4} \left([Ad_i] C_c [Ad_i]^\mathrm{T} \right)^{-1} \right)^{-1}, \tag{8}$$

which can be re-written in the form as

$$C_{2-\mathrm{DOS}} = \begin{pmatrix} c_{11} & 0 & 0 & 0 & c_{15} & 0 \\ 0 & c_{22} & 0 & c_{24} & 0 & 0 \\ 0 & 0 & c_{33} & 0 & 0 & 0 \\ 0 & c_{42} & 0 & c_{44} & 0 & 0 \\ c_{51} & 0 & 0 & 0 & c_{55} & 0 \\ 0 & 0 & 0 & 0 & 0 & c_{66} \end{pmatrix}. \tag{9}$$

By analyzing the principal diagonal elements of the matrix, the type of degree of freedom of this flexure mechanism can be easily demonstrated. In addition, other non-principal diagonal compliance entries can be considered as the reference of parasitic motion errors [21].

Table 1 Information for adjoint transformation

Beam number	Rotational matrix	Translational vector
1	$\boldsymbol{R}_1 = \boldsymbol{R}_x(\theta)$	$\boldsymbol{t}_1 = (-d, -a/a2.2, -a\cot(\theta))^{\top}$
2	$\boldsymbol{R}_2 = \boldsymbol{R}_x(-\theta)$	$\boldsymbol{t}_2 = (-d, a/a2.2, -a\cot(\theta))^{\top}$
3	$\boldsymbol{R}_3 = \boldsymbol{R}_x(\theta)$	$\boldsymbol{t}_3 = (d, -a/a2.2, -a\cot(\theta))^{\top}$
4	$\boldsymbol{R}_4 = \boldsymbol{R}_x(-\theta)$	$\boldsymbol{t}_4 = (d, a/a2.2, -a\cot(\theta))^{\top}$

Note that each entry in the compliance matrix of the 2-DoS mechanism is determined by the material and geometric properties, such as the cross-section radius of wire beam, the angle between two intersecting beams. Therefore, it is difficult to write the expressions of all entries explicitly. Luckily, enlightened by the combination with screw theory and kinematics, the form of overall compliance matrix reveals whether there is parasitic motion or not. Thus, in the initial qualitative preliminary analysis, we only focus on the form of each overall compliance matrix. As a result, the overall compliance matrices, with respect to the corresponding defined global coordinate frames, of other flexure mechanisms (Figure 9(a), 9(b) and 9(d)) are represented below and Eqs. (9)–(12) are normalized using the method in Ref. [16]. In this way, the deformations can sum up together in different dimensions because of the dimensionless processing.

$$\mathbf{C}_{0-\mathrm{DOS}} = \begin{pmatrix} c_{11} & c_{12} & 0 & c_{14} & c_{15} & 0 \\ c_{21} & c_{22} & 0 & c_{24} & c_{25} & 0 \\ 0 & 0 & c_{33} & 0 & 0 & c_{36} \\ c_{41} & c_{42} & 0 & c_{44} & c_{45} & 0 \\ c_{51} & 0 & c_{53} & c_{54} & c_{55} & 0 \\ 0 & 0 & c_{63} & 0 & 0 & c_{66} \end{pmatrix}, \quad (10)$$

$$\mathbf{C}_{1-\mathrm{DOS}} = \begin{pmatrix} c_{11} & 0 & 0 & 0 & c_{15} & c_{16} \\ 0 & c_{22} & c_{23} & c_{24} & 0 & 0 \\ 0 & c_{32} & c_{33} & c_{34} & 0 & 0 \\ 0 & c_{42} & c_{43} & c_{44} & 0 & 0 \\ c_{51} & 0 & 0 & 0 & c_{55} & c_{56} \\ c_{61} & 0 & 0 & 0 & c_{65} & c_{66} \end{pmatrix}, \quad (11)$$

$$\mathbf{C}_{3-\mathrm{DOS}} = \begin{pmatrix} c_{11} & 0 & 0 & 0 & 0 & 0 \\ 0 & c_{22} & 0 & 0 & 0 & 0 \\ 0 & 0 & c_{33} & 0 & 0 & 0 \\ 0 & 0 & 0 & c_{44} & 0 & 0 \\ 0 & 0 & 0 & 0 & c_{55} & 0 \\ 0 & 0 & 0 & 0 & 0 & c_{66} \end{pmatrix}. \quad (12)$$

According to all the above overall compliance matrices, it can be concluded that the smaller parasitic motion errors occurs when there are more symmetric planes existing in the flexure mechanisms. In other words, the DoS of a flexure mechanism leads to some straightforward effect on its parasitic motion error. It is worth mentioning that all these flexure mechanisms have the same

dominant motion pattern which consists of a rotation about the x axis (θ_x) and a translation along the x axis (δ_x).

3.3 Parasitic Motion Error Analysis

Now, let us take a close look at the overall compliance matrix formula of each flexure mechanism when a force f_x is imposed on the mobile platform. According to the screw theory and the theory of linear elasticity, the deformation denoted by the twist $\boldsymbol{\xi} = (\boldsymbol{\theta}; \boldsymbol{\delta}) = (\theta_x, \theta_y, \theta_z; \delta_x, \delta_y, \delta_z)$ and the load wrench $\boldsymbol{F} = (\boldsymbol{\tau}; \boldsymbol{f}) = (\tau_x, \tau_y, \tau_z; f_x, f_y, f_z)$ are connected by the generic 6×6 compliance matrix, written as

$$\begin{pmatrix} \theta_x \\ \theta_y \\ \theta_z \\ \delta_x \\ \delta_y \\ \delta_z \end{pmatrix} = \begin{pmatrix} c_{11} & c_{12} & c_{13} & c_{14} & c_{15} & c_{16} \\ c_{21} & c_{22} & c_{23} & c_{24} & c_{25} & c_{26} \\ c_{31} & c_{32} & c_{33} & c_{34} & c_{35} & c_{36} \\ c_{41} & c_{42} & c_{43} & c_{44} & c_{45} & c_{46} \\ c_{51} & c_{52} & c_{53} & c_{54} & c_{55} & c_{56} \\ c_{61} & c_{62} & c_{63} & c_{64} & c_{65} & c_{66} \end{pmatrix} \begin{pmatrix} \tau_x \\ \tau_y \\ \tau_z \\ f_x \\ f_y \\ f_z \end{pmatrix}, \quad (14)$$

where the parameters in the compliance matrix are normalized for summing up deformations together reasonably.

Considering the first case without symmetric plane (0-DoS mechanism), there exists such a resulting deformation, expressed as

$$\xi_0 = \theta_x + \theta_y + \delta_x + \delta_y = c_{14}f_x + c_{24}f_x + c_{44}f_x + c_{54}f_x.$$

In fact, only the translational motion along x-axis is useful to perform desired function, the rest of entries are unwanted since they bring into some parasitic motions. In this case, the moving platform translates by δ_x along x direction, companying with three other parasitic motions, which are two parasitic rotations about x and y axes, denoted by θ_x and θ_y respectively, and a parasitic translation along y axis, denoted by δ_y. As known, parasitic motion is always detriment to the accuracy of a flexure mechanism, Clearly, this 0-DoS mechanism is not desired for practical application.

As for the second case (1-DoS mechanism), it has one *yoz* symmetrical plane. Based on the matrix obtained above, the resulting deformation is deduced as

$$\xi_1 = \theta_y + \theta_z + \delta_x = c_{24}f_x + c_{34}f_x + c_{44}f_x.$$

The preliminary motion for translation along x axis remains unchanged, but the number of parasitic motions decreases into two that are the parasitic rotations about y and z axes, denoted by θ_y and θ_z, respectively. Comparing with the former 0-DoS case, the presence of one symmetrical plane leads to better performance due to eliminating one type of parasitic motion.

For the third case, it has the widest popularity when designing 2-DOF cylindrical flexure mechanisms. There

He *et al. Chin. J. Mech. Eng.* (2018) 31:29

Page 8 of 12

are a number of related literatures that address how to eliminate parasitic motion. Most of them claim that the introduction of a compensation module can effectively tradeoff the unwanted parasitic motion error. With the above-mentioned result, the flexure mechanism with two symmetric planes also has parasitic motion, but shows improvement when comparing with the 0-DoS and 1-DoS mechanisms. The resulting deformation of the 2-DoS mechanism is expressed as $\xi_2 = \theta_y + \delta_x = c_{24}f_x + c_{44}f_x$.

As can be seen, the best design should be the last one, whose overall compliance matrix is ideally pure diagonal. This is because all symmetric planes result in the advantage of no parasitic motion. Though it is challenging to design a 3-DoS flexure mechanism from all selected motion type, the attempt to design flexure mechanisms with maximum degree of symmetry is still meaningful.

4 FEA Simulation Verification

In this section, a series of finite element analysis (FEA) simulations are implemented for demonstrating the benefit in presence of more symmetrical planes in the flexure mechanism. The tool used is commercial package ANSYS 15.0, where SOLID-187 element is selected for all rigid platforms while BEAM-189 element is selected for all flexure beams which connecting the moving platform with the fixed platform.

Flexure mechanisms with different mobility and stiffness can be obtained by changing their geometrical parameter. The chosen material is Aluminum Alloy, whose Young's modulus is $E = 70$ GPa, Poisson's ratio is $\mu = 0.34$, and the cross-section radius of all wire flexures in the mechanisms is $r = 5$ mm. To guarantee the ratio of the length to the radius to be larger than 40, the height between the moving platform and the fixed one should at least be 200 mm. Thus, the length of the platform, which is also the distance a as shown in Figure 8 is 60 mm. The interval distance d is also set to be 60 mm.

Four models that have different number of DoS ranging from zero to three are built in terms of the geometrical parameters provided above. When applying the same force $f_x = 0.01$ N to the moving platform of four flexure mechanisms, they generate a deformation twist along x axis companied by several parasitic motion, which lead to inequality between the maximum displacement (DMX) displaying on the panel of Nodal Solution and the selected directional displacement (SMX) displaying on the panel of Nodal Solution. Therefore, the difference of DMX and SMX can be used as an indication of parasitic motion for these four designs. All corresponding deviations generated by the simulation results shown in Figure 10 are illustrated in Figure 11. It can be concluded that the higher the DoS, the smaller the parasitic motion error.

5 Optimal Parametric Design

Analyzing overall compliance matrix for different flexure mechanisms in Section 3, it is known that the resultant mechanism with three symmetric planes can lead to no parasitic motion theoretically because of its diagonal compliance matrix form. As a result, in this section we considerately concentrate on the optimization design for the 3-DoS flexure mechanism and find out the effect of design parameters on its compliance matrix, whose entries are considered as the reference of rational and translational DOF or DOC.
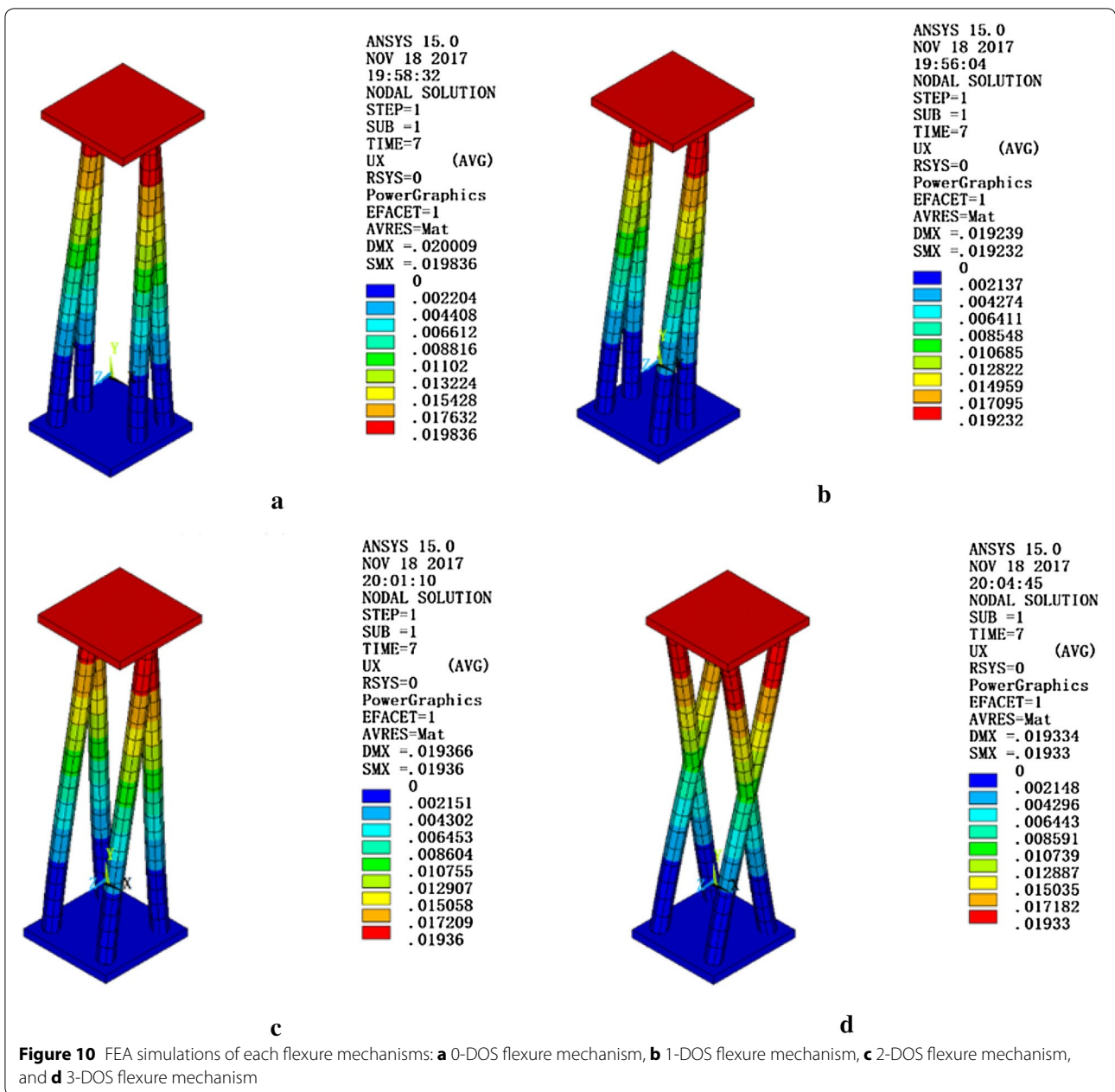
In this case, the entry c_{11} and c_{44}, in the diagonal should be the dominant ones for ensuring a rotation along the x-axis and a translational about the y-axis. Quantitatively, these two entries that have been already normalized should be much larger than the other entries in the diagonal. The much larger the ratio of the DOF entry to the DOC entry is, the better the kinetostatic characteristic of the mechanism is. For this reason, we derive symbolically every entry by four parameters (d, a, θ, r) as below:

$$
\begin{cases}
c_{11} = \frac{a}{E\pi r^4 \sin\theta}, \\
c_{22} = a^3/[\pi r^2 \sin\theta (2Ga^2 r^2 \sin^2\theta + 12Ed^2 r^2 \sin^4\theta + \\
\quad Ea^2 r^2 \cos^2\theta + 4Ea^2 d^2 \cos^2\theta)], \\
c_{33} = a^3/[\pi r^2 \sin\theta (2Ga^2 r^2 \cos^2\theta + Ea^2 r^2 \sin^2\theta + \\
\quad 12Ed^2 r^2 \cos^2\theta \sin^2\theta + 4Ea^2 d^2 \sin^2\theta)], \\
c_{44} = \frac{a^3}{12E\pi r^4 \sin^3\theta}, \\
c_{55} = \frac{a^3}{4E\pi r^2 \sin^3\theta (3r^2 \cos^2\theta + a^2)}, \\
c_{66} = \frac{a^3}{4E\pi r^2 \sin\theta (3r^2 \sin^4\theta + a^2 \cos^2\theta)},
\end{cases}
$$

where E is the Young's modulus, G is the shear modulus.

First of all, the compliance ratios (c_{11}/c_{22}, c_{11}/c_{33}, c_{44}/c_{55}, c_{44}/c_{66}) are plotted in Figures 12 and 13. The two figures illustrate the effect of the beam orientation (θ) on the compliant ratios, associating with the rotational DOF about the x-axis and the translational DOF along the x axis. It is shown that with the increase of the angle of beam orientation, the compliance ratios c_{11}/c_{22} and c_{44}/c_{66} both decrease. This result suggests that the compliance for rotational motion about the y-axis becomes notable, so does the translational motion along the z-axis. It can be understood that the original flexure mechanism will evolve into a new flexure mechanism with 2 extra DOFs including rotation about y-axis and translation along z-axis. In Figures 12 and 13, except two downward lines, there is one upward line and one almost steady line, indicating the constraint capacity against freedom capacity. It is a common sense that the compliance in the DOC direction should be small enough while as large as possible in the DOF direction. Therefore, the trend in compliance ratio c_{11}/c_{33} towards better rotational constraint.

He *et al. Chin. J. Mech. Eng.* (2018) 31:29

Page 9 of 12

Figure 10 FEA simulations of each flexure mechanisms: **a** 0-DOS flexure mechanism, **b** 1-DOS flexure mechanism, **c** 2-DOS flexure mechanism, and **d** 3-DOS flexure mechanism

For the value of compliance ratio c_{44}/c_{55}, almost constant larger than 50, can be referred to a translational DOF along the x-axis.

Based on the illustrated analysis above and in view of the design purpose for this paper, $\theta = \pi/4$ is selected to enable all compliance ratios to be large enough for better performance, so that we can obtain relatively high compliance in the specified DOF direction and relatively low compliance in the specified DOC direction.

Then, we focus on the effect of the distance a on the compliant ratios associating with the two desired DOFs.

The compliance ratios (c_{11}/c_{22}, c_{11}/c_{33}, c_{44}/c_{55}, c_{44}/c_{66}) are plotted against the distance a in Figures 14 and 15. Figure 14 shows that as the distance of intersecting beams increases, the compliance ratios c_{11}/c_{22} and c_{11}/c_{33} both decrease to approximate 288. It means that c_{22} and c_{33} are still two orders of magnitude smaller than the compliance c_{11} so that they can be reasonably neglected for the qualitative study. On the contrary, the compliance ratio c_{44}/c_{55} rises when the distance a increases, and the compliance ratios c_{44}/c_{66} is independent of the parameter a.
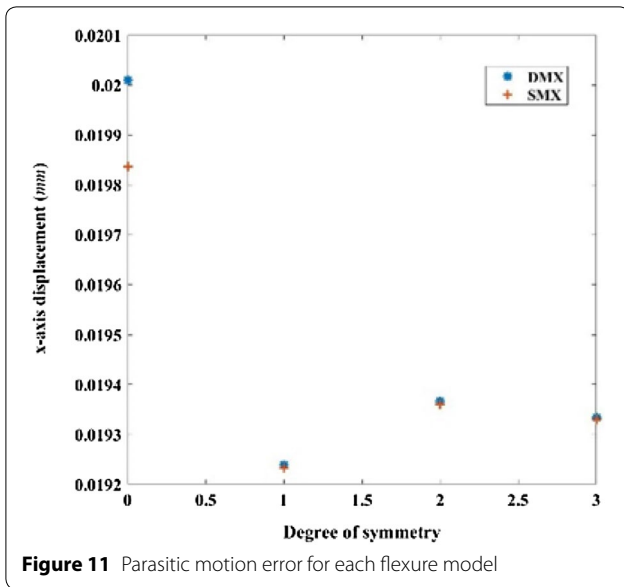
He *et al. Chin. J. Mech. Eng.* (2018) 31:29

Page 10 of 12

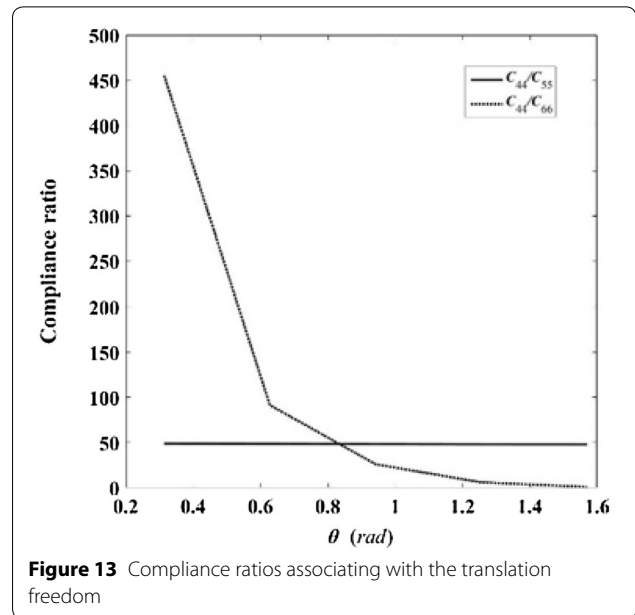**Figure 11** Parasitic motion error for each flexure model

Figure 13 Compliance ratios associating with the translation freedom
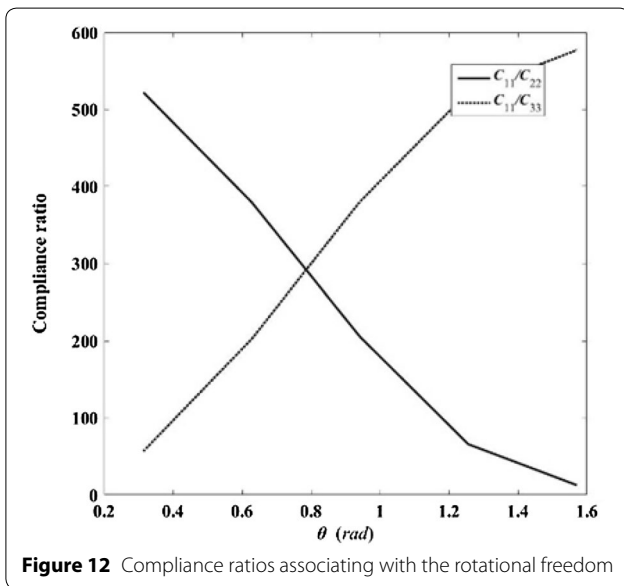

Figure 12 Compliance ratios associating with the rotational freedom

The effect of the interval distance d on the compliant ratios is further investigated. From the expression of the compliance matrix, the parameter d only affects c_{22} and c_{33} with same upward trend. Moreover, as shown in Figure 16, under $\theta = \pi/4$, c_{11}/c_{22} ad c_{11}/c_{33} are identical with the change of b.

Finally, the influence of the cross-section radius of beams is analyzed. Since the equivalent constraint model subjects to its ratio of the length to the radius, for the equivalent wire constraint model as used in this paper, there is no doubt that the smaller the radius of the beam is, the more ideal the wire flexure approximation is.

Nevertheless, significantly reducing the radius of flexure beam is not economic because of the manufacturing cost.

On the basis of the above comprehensive quantitative analysis, the optimal parameters for the 3-DoS mechanism are listed in Table 2. The FEA simulation is also implemented using the optimal parameters under the same force $f_x = 0.01$ N, showing that the value of DMX is equal to the value of SMX (Figure 17). Compared to the simulations in Section 4, the displacement along x axis after optimization is about two times larger than the original one. With the optimal parameters, the flexure mechanism is less stiff and lower power consumption.

6 Discussions

As mentioned in Section 1, there are mainly three methods to reduce or even eliminate the parasitic motion for a flexure mechanism. Compensation designs are always preferred as reported by numerous literatures, which can be simply constructed with high accuracy by mirroring two identical flexure modules. In a word, almost all existing flexure mechanisms use the principle of symmetry design and combinations of the homogenous modules to achieve the compensation for parasitic motion. In the design processing, it is better to generate as many DoS as possible from the very beginning based on the findings in this paper. With different DoS, we can further adopt certain methods to alleviate the unwanted parasitic motion.

In addition, design and synthesis of a class of flexure mechanisms with cylindrical motion in a compact but simple way is significant for further applications, such as the joint for realizing a snack-like robot's three
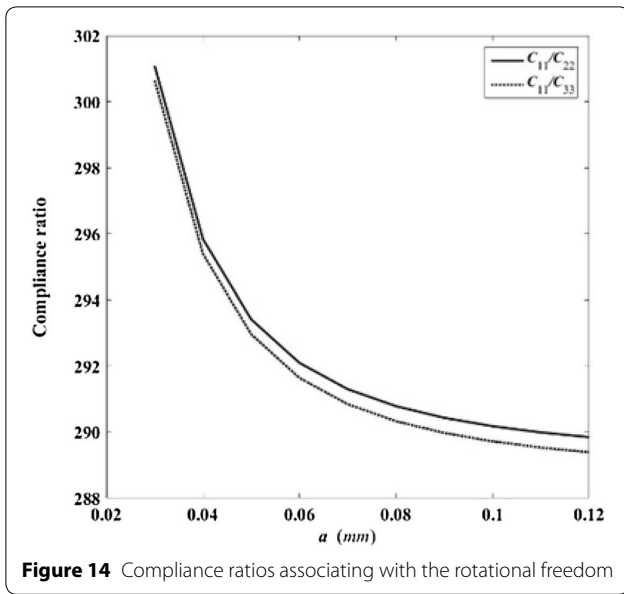
He *et al. Chin. J. Mech. Eng. (2018) 31:29*

Page 11 of 12

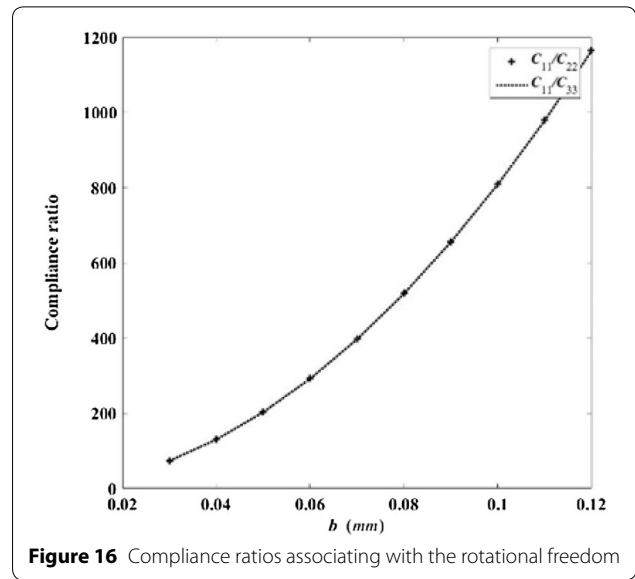**Figure 14** Compliance ratios associating with the rotational freedom

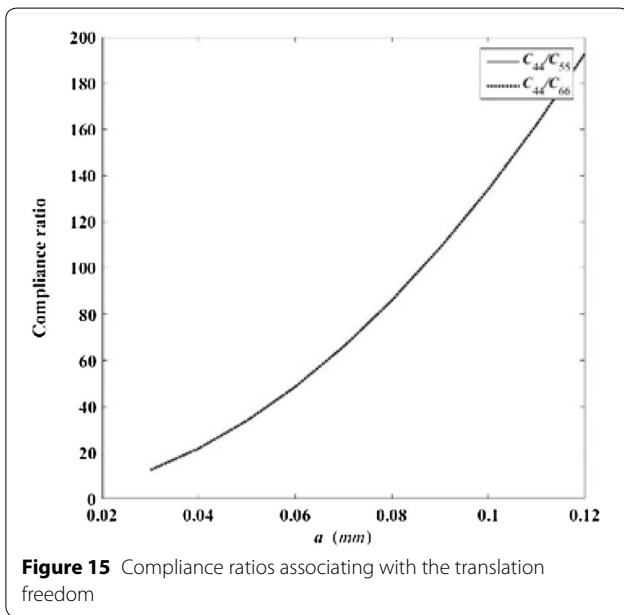**Figure 16** Compliance ratios associating with the rotational freedom

Figure 15 Compliance ratios associating with the translation freedom

Table 2 Optimal parameters for 3-DoS flexure model

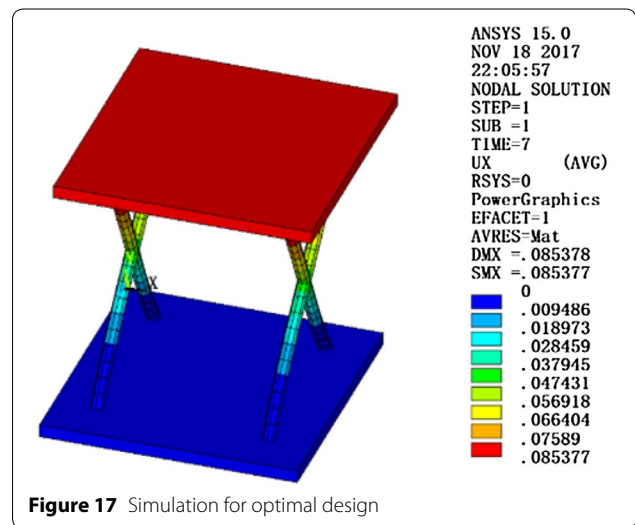| Beam orientation θ	Two end points distance a (mm)	Interval distance d (mm)	Radius of beam r (mm)
$\theta = \pi/4$	200	200	5

Figure 17 Simulation for optimal design

dimensions' gaits [24]. Recently, a new version of robots called in-pipe inspection robots was proposed to investigate the internal space of the pipes (for detecting the cracks, leaks, etc.), where implementing non-destructive tests are commonly based on screw motion [25]. As known, in-pipe inspection robots are supposed to move fast and continuous with constant pitch of rate, and it is possible because of cylindrical locomotion with the required accuracy.

7 Conclusions

A class of flexure mechanisms with different number of DoS have been designed followed by discussing the effect of symmetrical geometry on their kinetostatic characteristics. These mechanisms with zero, one or more symmetric planes, are obtained from FACT method.

He *et al. Chin. J. Mech. Eng.* (2018) 31:29

Page 12 of 12

Each flexure mechanism is composed of several identical beams distributed in two planes orthogonal to the motion direction. Analytical model for the overall compliance matrix has been derived within the framework of the screw theory. These models have been used to analyze the influences of different DoS on the parasitic motion. Moreover, the FEA simulations are carried out for verifying the analytical results. An optimal design with $\theta = \pi / 4$ and $a = d = 200$ mm has been obtained and simulated.

As a new concept, the DoS concentrates on symmetry design theory. Moreover, the comparative case study on designing a group of symmetrical flexure mechanisms with cylindrical motion is instructive to snack-like robots' design.

Additional file

Additional file 1. Brief introduction of the paper.

Authors' Contributions
J-JY was in charge of the whole trial; X-BH, G-BH wrote the manuscript; W-WZ assisted with sampling and laboratory analyses. All authors read and approved the final manuscript.

Author details
¹ School of Mechanical Engineering and Automation, Beihang University, Beijing 100191, China. ² School of Engineering-Electrical and Electronic Engineering, University College Cork, Cork, Ireland.

Authors' Information
Xiao-Bing He, born in 1994, is currently a master candidate at *School of Mechanical Engineering and Automation, Beihang University, China*. E-mail: 18811375101@163.com.

Jing-Jun Yu, born in 1974, is currently a professor at *Beihang University, China*. His research interests include mechanisms and robotics. Tel: +86–10–82313904; E-mail: jjyu@buaa.edu.cn.

Wan-Wan Zhang, born in 1994, is currently a master candidate at *School of Mechanical Engineering and Automation, Beihang University, China*. E-mail: 1076643918@qq.com.

Guang-Bo Hao, born in 1981, is currently a permanent full-time Lecturer in Mechanical Engineering at *School of Engineering-Electrical and Electronic Engineering, University College Cork (UCC), Ireland*. His research focuses on compliant mechanisms.

Competing Interests
The authors declare that they have no competing interests.

Ethics Approval and Consent to Participate
Not applicable.

Publisher's Note
Springer Nature remains neutral with regard to jurisdictional claims in published maps and institutional affiliations.

References
[1] L L Howell. Compliant mechanisms. In: *21st Century Kinematics.* London: Springer, 2013: 457–463.
[2] R M Panas, J B Hopkins. Eliminating underconstraint in double parallelogram flexure mechanisms. *Journal of Mechanical Design*, 2015, 137(9): 092301.
[3] L L Howell, B M Olsen, S P Magleby. *Compliant mechanisms.* New York: Wiley, 2001.
[4] L L Howell, et al. *Handbook of compliant mechanisms*. Chichester, West Sussex, United Kingdom: Wiley, 2013.
[5] G B Hao, J J Yu, H Y Li. A brief review on nonlinear modelling methods and applications of compliant mechanisms. *Frontiers of Mechanical Engineering*, 2016, 11(2): 119–128.
[6] S Awtar, A H Slocum. Constraint-based design of parallel kinematic XY flexure mechanisms. *ASME Journal of Mechanical Design*, 2006, 129(8): 816–830
[7] Q Li, J M Hervé. 1T2R parallel mechanisms without parasitic motion. *IEEE Transactions on Robotics*, 2010, 26(3): 401–410.
[8] Q Li, Z Chen, Q Chen, et al. Parasitic motion comparison of 3-PRS parallel mechanism with different limb arrangements. *Robotics and Computer-Integrated Manufacturing*, 2011, 27(2): 389–396.
[9] S Z Li, J J Yu, G H Zong, et al. A compliance-based compensation approach for designing high-precision flexure mechanism. *ASME 2012 International Design Engineering Technical Conferences and Computers and Information in Engineering Conference*. New York: American Society of Mechanical Engineers, 2012: 293–301.
[10] Y M Moon, B P Trease, S Kota. Design of large-displacement compliant joints. *ASME 2002 International Design Engineering Technical Conferences and Computers and Information in Engineering Conference*, 2002: 65–76.
[11] B R Cannon, T D Lillian, S P Magleby, et al. A compliant end-effector for microscribing. *Precision Engineering*, 2005, 29(1): 86–94.
[12] N B Hubbard, J W Wittwer, J A Kennedy, et al. A novel fully compliant planar linear-motion mechanism. *International Design Engineering Technical Conferences and Computers and Information in Engineering Conference*, ASME, 2004: 1–5.
[13] S Z Li, J J Yu. Design principle of high-precision flexure mechanisms based on parasitic-motion compensation. *Chinese Journal of Mechanical Engineering*, 2014, 27(4): 663–672.
[14] G B Hao, F K Dai, X Y He, et al. Design and analytical analysis of a large-range tri-symmetrical 2R1T compliant mechanism. *Microsystem Technologies*, 2017(8): 1–8.
[15] G B Hao. Determinate synthesis of symmetrical, monolithic tip-tilt-piston flexure stages. *Journal of Mechanical Design*, 2017, 139(4): 042303–042303–9.
[16] G B Hao. Design and analysis of symmetric and compact 2R1T (in-plane 3-DOC) flexure parallel mechanisms. *Mechanical Sciences*, 2017, 8: 1–9.
[17] D L Blanding. *Exact constraint: Machine design using kinematic principle*. New York: ASME Press, 1999.
[18] J B Hopkins, M L Culpepper. Synthesis of multi-degree of freedom, parallel flexure mechanism concepts via freedom and constraint topology (FACT). Part II: Practice. *Precision Engineering*, 2010, 34(2): 271–278.
[19] J J Yu, S Z Li, H J Su, et al. Screw theory based methodology for the deterministic type synthesis of flexure mechanisms. *ASME Journal of Mechanisms and Robotics*, 2011, 3(3): 031008.
[20] J B Hopkins, M L Culpepper. A screw theory basis for quantitative and graphical design tools that define layout of actuators to minimize parasitic errors in parallel flexure systems. *Precision Engineering*, 2010, 34(4): 767–776.
[21] R Murray, Z X Li, S Sastry. *A mathematical introduction to robotic manipulation*. New York: CRC Press, 1994.
[22] G B Hao, X W Kong. A normalization-based approach to the mobility analysis of spatial compliant multi-beam modules. *Mechanism and Machine Theory*, 2013, 59(1): 1–19.
[23] H J Su, H J Shi, J J Yu. A symbolic formulation for analytical compliance analysis and synthesis of flexure mechanisms. *ASME Journal of Mechanical Design*, 2011, 134(5): 051009.
[24] B Klaassen, K L Paap. GMD-SNAKE2: A snake-like robot driven by wheels and a method for motion control. *IEEE International Conference on Robotics and Automation, 1999. Proceedings*. IEEE Xplore, 1999, 4: 3014–3019.
[25] A Nayak, S K Pradhan. Design of a new in-pipe inspection robot. *Procedia Engineering*, 2014, 97: 2081–2091.